International Journal of Hydrogen Energy 49 (2024) 747–757

Contents lists available at ScienceDirect

International Journal of Hydrogen Energy

journal homepage: www.elsevier.com/locate/he

Characterisation of turbulent non-premixed hydrogen-blended flames in a scaled industrial low-swirl burner

Adam J. Gee [a,*], Neil Smith [b], Alfonso Chinnici [a], Paul R. Medwell [a]

[a] School of Electrical and Mechanical Engineering, The University of Adelaide, Adelaide, SA, 5005, Australia
[b] School of Chemical Engineering and Advanced Materials, The University of Adelaide, Adelaide, SA, 5005, Australia

ARTICLE INFO

Handling editor: Dr Mehran Rezaei

Keywords:
Hydrogen
Low-swirl
Burner
Non-premixed
Turbulent

ABSTRACT

The performance of a scaled industrial, non-premixed, low-swirl burner design was experimentally investigated for hydrogen addition to natural gas. Two strategies for introducing hydrogen are considered, namely, conserving (i) heat input and (ii) velocity/volumetric flow of the original fuel. This work characterises the effects on key performance metrics of the burner as hydrogen fraction is increased. Compared with natural gas, the results with hydrogen showed a 33 % reduction in the radiant fraction and up to a 380 % increase in NOx emissions. The lift-off height was reduced by a maximum of 23 % and 51 % for addition of 10 and 30 vol% hydrogen addition, respectively, with 100 % cases becoming completely attached to the burner. The influence of hydrogen-addition strategy and air adjustment was shown to be significant with respect to NOx emissions but less significant than the resulting changes in fuel composition and heat input with respect to flame appearance, stability and radiant heat transfer.

1. Introduction

Hydrogen has gained considerable attention in recent years as the world continues to look toward alternative energy sources. The potential of a renewable production process and zero carbon emissions make hydrogen an ideal candidate as an alternative to fossil fuels. In particular, hydrogen is a strong candidate for partial or complete substitution with fuels such as natural gas in a variety of domestic and industrial combustion applications, especially those which are not well suited for electrification. Unknowns about the method and magnitude by which hydrogen impacts the performance of current gas appliances are a significant risk faced by end-users, appliance manufacturers, and regulators.

High-temperature, direct-fired combustion applications such as those used in iron pelletising, cement and glass manufacturing are all well-suited for hydrogen adoption. Operating existing burners on fuels for which they were not designed is challenging, especially for fuels such as hydrogen, which has vastly different combustion characteristics to natural gas. Common features of these burners, such as swirling flows, create added difficulty when attempting to accurately predict the outcomes of using hydrogen as a complete or partial fuel alternative. Furthermore, the addition of hydrogen has the potential to alter critical flame characteristics such as heat transfer on which the industry relies, and to alter emissions. The geometric complexities of the kilns and furnaces further add to the challenge.

Swirl geometry is commonly incorporated into the design of industrial burners to improve performance via enhanced fuel/air mixing and increased flame stability. Fundamentally, swirl burners reduce the axial momentum of the flow after it leaves the burner by introducing a tangential momentum component to fuel and/or air streams by using either a series of tangential inlet jets or swirl vanes. Swirl burner flames can be broadly classified into two categories: high-swirl burners (HSB) and low-swirl burners (LSB). A variety of factors differentiate HSB and LSB in practical applications, most notably, the fraction of stoichiometric air commonly supplied through the burner. HSB are typically supplied with most, if not all, the required stoichiometric air, whereas LSB flames have only a small fraction of primary air supplied, with the remainder from secondary sources. A fundamental distinction between LSBs and HSBs is the recirculation characteristics and flame-stabilisation mechanisms [1,2]. HSB flames induce a vortex-breakdown which forms a strong recirculation of reactants and hot combustion products which stabilises the flame [1,3], as swirl intensity increases air entrainment and flame length are typically increased and decreased, respectively [4]. In LSB flames, the swirl is not large enough to induce vortex-breakdown and the resulting recirculating flows, instead stability is achieved by

* Corresponding author.
E-mail address: adam.gee@adelaide.edu.au (A.J. Gee).

https://doi.org/10.1016/j.ijhydene.2023.11.164
Received 21 August 2023; Received in revised form 10 October 2023; Accepted 13 November 2023
Available online 22 November 2023

Nomenclature

HSB	High swirl burner
LSB	Low swirl burner
d	diameter
Re	Reynolds number
S	Swirl number
R_h	Hub radius
R_s	Swirl radius
θ	Vane angle
HAB	Height above burner
Q_r	Radiant heating fraction
Q_s	Heat flux
Q_t	Total heat input
R	Distance from flame centreline to sensor
LHV	Lower heating value
HHV	Higher heating value
$\dot{m}$	Mass flow rate
m	Mass
EI	Emission Index
U	Velocity
V	Volumetric flow rate
ρ	density
φ	Equivalence ratio

creating a low-velocity region [1,3,5]. Due to this mechanism of stabilisation, typical LSB flames are often lifted (detached) from the burner surface, and consequently, the turbulent burning velocity of the fuel is a critical parameter [6,7]. Although a lifted flame can be useful for keeping burner surface temperatures low, lifted flames have a high susceptibility to blow-off. This can be a limiting factor when trying to maximise energy input via a high flow rate of fuel [1,3].

Much of the available work on hydrogen addition to non-premixed LSB considers temperature and NOx emissions, as these are major challenges for hydrogen adoption in the context of industrial combustion. Hydrogen addition to an industrial low-swirl burner has been shown to cause an increase in peak flame temperatures, most notably in the initial portion of the flame, which caused significant increases in NOx emissions [8]. For the hydrogen natural gas fuel blends, the majority of NOx emissions were shown to be formed via the thermal pathway. For blends containing 25 %, 50 %, 75 % and 100 % hydrogen (as a fraction of total heat input) resulting in NOx emission increases of 93 %, 220 %, 360 %, 486 % respectively [8]. Others have reported similar increases in NOx and flame temperature in non-premixed swirl burners, in addition to reductions in soot [9,10] and shrinking of the swirl recirculation zones [11] all of which were associated with hydrogen addition.

The role of soot is critically important in practical combustion applications, which depend on radiation as a primary mode of heat transfer. Carbonaceous soot particles are responsible for the majority of the radiant heat transfer and contribute significantly to the luminosity of hydrocarbon flames [12–18]. The displacement of carbon-based fuels to reduce carbon emissions can have undesirable consequences to the heat transfer efficiency of flames.

The location of fuel supply has also been shown to be a contributing factor the performance of hydrogen-blended flames in co-annular burners. NOx emissions are reported much higher when hydrogen is added to the outer annulus of a co-annular burner, compared to the inner annulus [11]. The underlying cause for these effects was deduced to be due to the enhanced or inhibited capacity for diffusion of air into the reaction zone, coupled with the increased diffusibility of hydrogen compared with natural gas. In the same study [11], supplying fuel through the inner annulus caused the recirculation zone to shrink compared with the outer or both annuli.

The impact of hydrogen addition on swirl structure and resulting fuel/air mixing and residence time has been investigated previously [19–21] where it was shown that excess fuel-stream momentum can disrupt mixing and causes undesirable changes in properties such as heat radiation [19–21] and combustion stability [21]. This is especially relevant for non-premixed regimes, since the fuel/air mixing at the jet nozzle is highly sensitive to changes in stoichiometry which may come about by changes in mixing [20,21]. Some examples of practical implications of this on performance is shown via excessive wall heating due to the changes in flame length induced by excessive swirl [19] or increased NOx formation due to increases in residence time [3,22]. It is worth noting that some studies report blending with hydrogen can increase size and robustness of the reaction zone in non-premixed swirl burner flames, which may be desirable in industrial applications [23]. The influence of co-annular air supply on fuel/air mixing is an important parameter with respect to the combustion reaction, heat distribution and emissions [24–29]. A numerical study on the effect of swirling intensity on the NOx emissions in a methane-air flame showed how increasing the swirl intensity promotes a uniform temperature distribution a lower thermal NOx production [26]. Reduced peak flame temperatures and thermal NOx formation as a result of modification of the swirling co-annular air supply to optimise mixing at the jet exit have also been shown experimentally in non-premixed turbulent combustion in a rotary kilns [24,25].

Adjusting the co-annular air supply may be a simple and cost-effective approach to limit the impact of hydrogen addition. The lower energy density of hydrogen will impact fuel stream velocity and momentum flux, depending on which strategy is employed to add hydrogen (e.g. conservation of heat input) and the increased diffusivity of hydrogen can induce vortex breakdown in swirl burner flames [28]. The impact of hydrogen addition on swirling structures is well documented in the context of high-swirl or premixed flames [9,30,31] but less is known about the effects in non-premixed LSB flames.

The available literature on LSB flames has shown, as with other burners, hydrogen addition to LSB flames increases NOx emissions via the thermal route [8,11]. The effect of hydrogen on stability and swirl structure has been shown to be impacted in several ways via changes in fuel stream momentum [19–21], differential-diffusion [32,33] and burning velocity [34] as a result of hydrogen blending.

The influence of hydrogen addition and co-annular air adjustment strategies are not sufficiently addressed with respect to practical performance metrics in industrial burner designs. In particular, the addition of hydrogen has not been investigated in low-swirl, co-annular, dual-swirl designs. This gap in knowledge creates a risk for industries looking to adopt hydrogen which rely on this mode of operation. Metal/mineral processing, cement and glass manufacturing industries which utilise high-temperature, direct fired heating often feature swirl burner designs. More experimental work of this sort is required in order to continue to develop the models which will eventually be used to predict the outcomes of hydrogen addition to full-scale industrial combustors [35]. The co-annular air supply and swirled geometry play a crucial role in flame stabilisation, fuel/air mixing and system cooling in these applications. Many of these industries are potential candidates for hydrogen adoption but will require a more thorough investigation of the opportunities and challenges involved in a partial or full integration of hydrogen.

The novelty of this work is the bridging of the aforementioned gaps in understanding by experimentally investigating the effect of hydrogen addition to a scaled industrial low-swirl burner. Key performance criteria are quantified, in particular, flame appearance and lift-off behaviour, heat transfer characteristics and NOx emissions. The

quantification of these practical performance parameters for a turbulent, non-premixed, hydrogen-blended flame in a scaled industrial low-swirl burner provides a valuable insight to industrial applications which utilise this design.

2. Methods

2.1. Burner apparatus

The burner used for this investigation is depicted in Fig. 1 with dimensions specified in Table 1. It is a co-annular, low-swirl burner design, adapted from an industrial burner used in direct-fired, high-temperature combustion applications.

The burner was scaled down from 20 MW using constant velocity principles. The design was 3D printed from titanium and features two co-rotating swirled annular channels and a central bluff-body hub. In these experiments, fuel and air were supplied separately, with fuel supplied via the inner channel and air supplied via the outer channel. A geometric swirl number (S) is used to describe the geometry of the burner, following methods described by Cheng et al. [36]. The equation for geometric swirl number is presented in Eq. (1) where R_h and R_s are the hub and swirling radii, respectively, and θ is the swirl vane angle. In this case, the inner channel is calculated to be 0.77 using a 13.7 mm hub radius, 29 mm swirling radius and a 45° vane angle. Similarly, the outer swirl number is calculated to be 0.83 from a 29 mm hub radius, 47.3 mm swirling radius and a 45° vane angle.

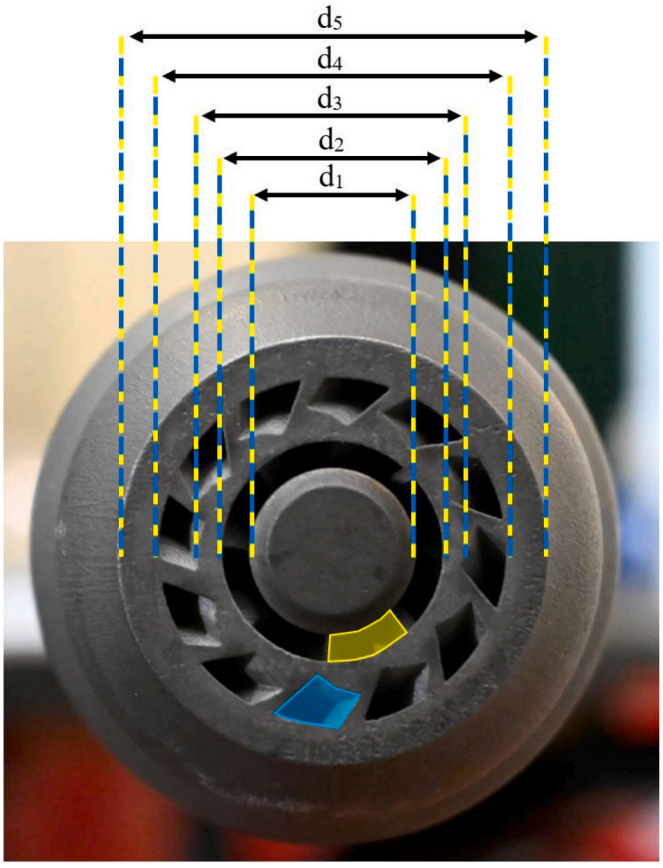

Fig. 1. *Photograph of the swirl nozzle used in this investigation, showing diameters of the central bluff-body hub* (d_1)*, inner swirled annulus* (d_1-d_2), outer swirled annulus (d_3-d_4) and outer wall outside diameter (d_5). *One of the fuel and air channels has also been highlighted* yellow *and blue, respectively*. (For interpretation of the references to colour in this figure legend, the reader is referred to the Web version of this article.)

Table 1
Burner specifications.

Measurement	Value
d_1	13 mm
d_2	17 mm
d_3	19 mm
d_4	27 mm
d_5	33 mm
Vane angle of fuel channel (θ)	45°
Vane angle of air channel (θ)	45°
Total area of fuel channels	91 mm^2
Total area of air channels	107 mm^2
No. of fuel channels	8
No. of air channels	12

$$S = \frac{2}{3}\left[\frac{1-(R_h/R_s)^3}{1-(R_h/R_s)^2}\right]\tan(\theta) \quad (1)$$

2.2. Experimental diagnostics

The diagnostic techniques used in this investigation are chosen to provide a global perspective of the impact of hydrogen addition to a scaled industrial swirl burner. Additionally, these diagnostic techniques are relevant performance metrics for the practical implementation of hydrogen in industry. Specifically, visual photography and OH* chemiluminescence imaging, axial heat flux, in-flame temperature and emission measurements are used to characterise the performance of this swirl burner for various hydrogen-natural gas fuel blends and air supply rates. Given the sparsity of experimental and numerical data on hydrogen addition to a co-annular LSB, a considerable effort was made in this investigation to collect experimental data in sufficient detail to be utilised for future CFD model development. All error ranges presented account for the measurement accuracy of the equipment used, these are specified in the figure captions as appropriate.

Flame images were captured with a Canon EOS 6D DSLR camera fitted with a 50-mm lens. All photographs are taken using a 10-s exposure time, $f/22$ aperture and a white balance of 4900 K. Although the visibility of pure hydrogen flames can be poor, hydrogen flames do emit a small amount of visible light, with previous work highlighting the pale red colouration of a pure hydrogen flame [37,38]. In this experiment, the visible emissions of the pure hydrogen flames were dominated by a bright orange colour. Orange colouration of hydrogen flames has been reported previously, where flame spectrometry data showed this was a result of a sodium impurity from the surrounding air [18,39–41]. The visible emission from sodium peaks at 589 nm. To eliminate this uncontrolled artefact, imaging was through a 594-nm (23-nm full-width at half maximum) notch filter to eliminate the orange colour.

A camera with an intensified charge-coupled device (ICCD) was used with a 50-mm, $f/3.5$ UV lens and 310-nm bandpass filter (FWHM = 10 nm) to capture chemiluminescence data of the OH* radical for each flame. The OH* species only occurs within the reaction zone of a flame, which allows for location and quantification of the flame front, eliminating the ambiguity associated with traditional photography. The OH* images are presented in green false colouration, to distinguish them from true-colour images. Height above burner (HAB) measurements are provided on all flame image figures to provide a sense of scale. Additionally, OH* chemiluminescence data is used to quantify the lift-off height of each flame. Based on techniques adapted from previous work [42–44], the flame boundary is defined as the point at which OH* chemiluminescence intensity is less than 15 % of the peak intensity. This allows for the quantification of flame lift-off height from the burner.

A Medtherm heat flux sensor was used to quantify the radiant heating energy from the flames. The sensor was positioned on a vertical traverse and fitted with a view restrictor to narrow the view angle to 20°. This allows for the isolation of individual sections of the flame,

providing greater resolution of the heat flux profile. Heat flux samples were collected axially along to flame by traversing the heat flux sensor up and down the length of the flame. A sampling range of 0–1200 mm above the burner was used with a total of six sample locations (every 200 mm). The background reading was subtracted from the raw data. Radiant heat fraction is calculated using a point-radiation assumption and Eq. (2), similar to previous work [45–47]. The radiant fraction (Q_r) is calculated as the sum of axial heat flux samples (Q_s) along the flame multiplied by the radiative area ($4\pi R^2$) and normalised by the total heat input from the fuel stream, given by the multiplication of lower heating value (LHV) and mass flow rate ($\dot{m}$) of the fuel. Here, R is the distance from the flame centreline to the sensor.

$$Q_r = \frac{4\pi R^2 \sum Q_{s,n}}{LHV \cdot \dot{m}} \tag{2}$$

A Testo 350 gas analyser was used to collect flue gas NOx emission samples in the post-flame region. Axial measurements were taken to confirm any variation was a result of dilution and not reacting samples. Unless specified otherwise, the NOx data presented here is sampled from 2000 mm above the burner. A water-cooled probe is used to collect gaseous samples. The raw data is processed using previously established methods [39] where the background reading on the day of collection is removed before being corrected to 0 % O_2 and converted to an emission index using Eq. (3) where m is the mass of some pollutant (e.g. NO_2) in the sample and HHV is the higher heating value of the fuel blend.

$$EI = \frac{m}{HHV} \tag{3}$$

In-flame temperature measurements were taken using a sheathed R-type thermocouple with an outer diameter of 1.5 mm. Sampling was done in 200 mm increments from 100 to 1200 mm above the burner exit plane. All temperature data presented has been corrected for radiation heat transfer using methods described previously [48].

2.3. Flame cases

The base case operating conditions specified in this investigation are derived from the typical operation of the full-scale burner which the present burner is modelled after, using constant velocity scaling. In these experiments, the base case is defined as natural gas supplied at a rate of 97 kW via the central channel. Air is supplied via the outer channel giving a fuel-to-air momentum ratio of 1.68 and an equivalence ratio of 14.4. All flames are operated in a vertical orientation, in an unconfined, open-air environment.

As hydrogen is blended with natural gas, the total fuel flow is adjusted to conserve either total heat input or fuel stream velocity/volumetric flow rate, as these are two likely strategies which hydrogen may be introduced to an existing burner system. For the purposes of this investigation, fuel and air supply channels are kept constant throughout the experiments (i.e. fuel supplied through inner swirled channel and air supplied through outer swirled channel). In the initial cases presented in Sections 3.1-3.3, volumetric air supply is kept constant as hydrogen is added. To characterise the effect of co-annular air supply, alternative scenarios are considered where air supply is adjusted to conserve either fuel/air momentum flux ratio or equivalence ratio as hydrogen content changes, data for these flames is presented in Section 3.4. The list of flame cases considered in this investigation is presented in Table 2. A case code is assigned to the different conditions by which hydrogen was added and air supply was adjusted. For all calculated values (e.g. Re) that require a diameter, a hydraulic diameter is used for the fuel and air channels respectively.

3. Results and discussion

3.1. Visual observations

A combination of DSLR and OH* chemiluminescence imaging is used to characterise how hydrogen addition impacts the flame colour, visibility, length and lift-off height. In this section (Section 3.1), images for different hydrogen concentrations at constant heat input and jet velocity are compared to each other and referenced to the base natural gas case (NG). Each respective fuel blend are presented as split images, with the left half representing hydrogen added at constant heat input and the right half representing hydrogen added at constant velocity, with a blue and white line used to show the splitting axis. The flames presented in the initial sections (Sections 3.1-3.3) are for hydrogen addition at either constant heat input or constant velocity (Q and U prefixes, respectively), with a fixed volumetric air supply (-NA cases). Filtered DSLR images are

Table 2
List of flames investigated, including hydrogen in natural gas vol%, heat input (Q_t), fuel velocity (U_{fuel}), air volumetric flow rate (V_{air}), fuel/air momentum flux ratio, equivalence ratio and total fuel/air Reynolds number (Re) of each fuel blend. Case code: 'Q' and 'U' are used for cases where hydrogen is added at constant heat input or constant velocity, respectively. 'NA', 'MF' and 'ER' are used for cases where air supply is not adjusted, adjusted to conserve fuel/air momentum flux ratio or adjusted to conserve equivalence ratio, respectively.

Case code	H_2 (vol%)	Q_t (kW)	U_{fuel} (m/s)	V_{air} (SLPM)	$(\rho U^2)_{fuel}$ / $(\rho U^2)_{air}$	φ	Re_{fuel} (× 10^3)	Re_{air} (× 10^3)
NG	0 (natural gas)	97	32	119	1.68	14.4	19.4	13.0
Q-NA	10	97	35	119	1.79	14.3	18.7	13.0
	30	97	40	119	1.98	14.0	17.8	13.0
	100	97	105	119	2.26	11.7	10.0	13.0
U-NA	10	91	32	119	1.52	13.3	17.4	13.0
	30	77	32	119	1.24	11.1	14.1	13.0
	100	29	32	119	0.21	3.5	3.02	13.0
Q-MF	10	97	35	122	1.68	14.4	18.7	13.3
	30	97	40	125	1.68	13.5	17.8	14.1
	100	97	105	138	1.68	10.1	10.0	15.1
U-MF	10	91	32	114	1.68	14.4	17.4	12.4
	30	77	32	108	1.68	13.5	14.1	11.2
	100	29	32	42	1.68	10.1	3.02	4.55
Q-ER	10	97	35	118	1.79	14.4	18.7	12.9
	30	97	40	116	1.91	14.4	17.8	12.6
	100	97	105	97	3.45	14.4	10.0	10.5
U-ER	10	91	32	110	1.79	14.4	17.4	12.0
	30	77	32	101	1.91	14.4	14.1	10.0
	100	29	32	29	3.45	14.4	3.02	3.18

presented in Fig. 2 for hydrogen addition to natural gas at 10, 30 and 100 %. Note that the exposure of the pure hydrogen flames has been increased by a factor of four for all pure hydrogen flame images to improve visibility.

The results in Fig. 2 show a reduction in flame length and visibility with hydrogen addition up to 100 %. The distinction between constant heat input (left-split) and constant velocity (right-split) flames with respect to visible flame length is negligible up to 10 vol% hydrogen. The difference in visible flame length increases to ~14 % and ~32 % for 30 and 100 % hydrogen cases. Complete substitution of natural gas for hydrogen resulting in a 33 % and 50 % reduction in visible flame length for constant heat input and constant velocity cases, respectively. The discrepancy in flame length between constant heat input and constant velocity cases is presumed to be a consequence of reduced heat input at constant velocity as hydrogen fraction increases — this also explains why the discrepancy is greater for larger fractions of hydrogen.

Regardless of whether heat input or velocity were conserved, hydrogen addition of 10 and 30 vol% had no appreciable effect on visibility and remained a distinctive yellow colouration attributed to luminosity from soot. The pure hydrogen flames appeared a pale red colour that was almost invisible to the naked eye, much fainter than the appearance depicted in Fig. 2. The reduced visibility of pure hydrogen flames has been reported previously [18,49,50] with the cause primarily associated with the absence of soot whose incandescence contributes the majority of luminosity in hydrocarbon flames.

Some noteworthy observations in the initial 300 mm portion of the flames presented in Fig. 2 are a colour shift from blue to yellow and a lifted/detached flame up to 30 vol%. The blue colour suggests a more well mixed fuel and air mixture [51–53]. This is consistent with the assumption that fuel-air mixing is greatest near the base of the flame where the co-annular air was injected and recirculation/swirl intensity is strongest. Axial temperature measurements for the constant velocity cases, discussed in Section 3.3, were also observed to peak at ~300 mm above the burner, supporting the hypothesis that fuel-air mixing is highest in this region.

A detached flame is a typical feature of a LSB flame which can limit the heat input that can be supplied without exceeding blow-off limits [1,3]. The flames in Fig. 2 were visibly detached from the burner during operation, maintaining a consistent lift-off height which reduced as hydrogen fraction increased. This is more clearly visualised in Fig. 3, which shows the OH* chemiluminescence images of the base of each flame. A similar lift-off observation to the DSLR images can be seen with the images of the OH* chemiluminescence — that is, a lifted flame

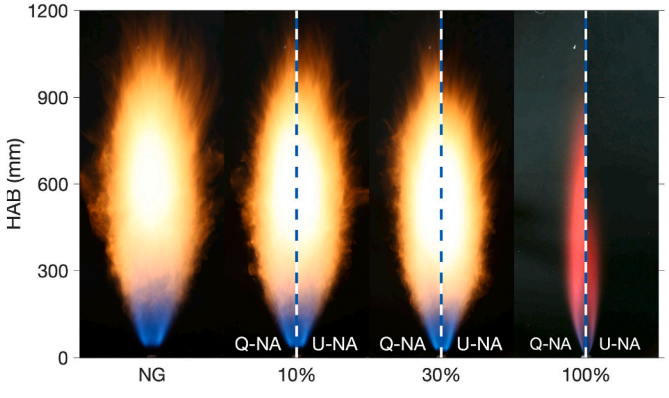

Fig. 2. Flame photographs for hydrogen addition to natural gas (NG) (v/v %) at either 0 % (NG), 10 %, 30 % or 100 % hydrogen. Photographs are split: (left) Q-NA for constant heat input and (right) U-NA for constant fuel-stream velocity. The volumetric flow rate of swirled co-annular air is not adjusted from the base case for all flames. HAB represents height above burner. Exposure time 10 s. Image intensity for the pure hydrogen flames has been increased four-fold to assist with visibility.

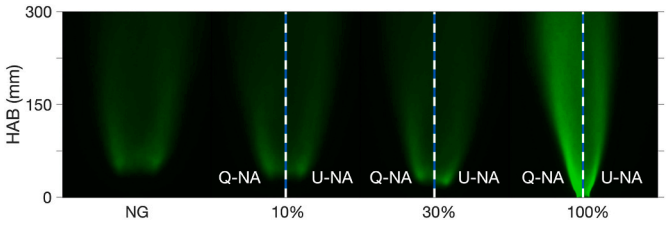

Fig. 3. OH* chemiluminescence images for hydrogen addition to natural gas (NG) (v/v %) at either 0 % (NG), 10 %, 30 % or 100 % hydrogen. Photographs are split: (left) Q-NA for constant heat input and (right) U-NA for constant fuel-stream velocity. The volumetric flow rate of swirled co-annular air is not adjusted from the base case for all flames. HAB represents height above burner. Exposure time 1 s. The image intensity of each flame was increased two-fold in postprocessing to assist with visibility.

which becomes reattached at 100 %. The pixel intensity from the images in Fig. 3 is used to quantify the lift-off heights from the burner for each flame using previously established techniques [42–44], as outlined in Section 2.2. The measured lift-off heights for each flame are presented in Fig. 4.

The results in Fig. 4 show a reduction in lift-off height with hydrogen addition of 10 and 30 vol% and attachment of the flame at 100 % hydrogen. The base natural gas flame is shown to be lifted 33 mm from the burner exit plane. Addition of hydrogen up to 10 vol% reduces the lift-off height by 21 % and 23 % depending on if heat input or velocity is conserved with hydrogen addition, respectively. Further addition of up to 30 vol% results in a 38 % and 51 % decrease relative to the base case, depending on if heat input or velocity is conserved with hydrogen addition, respectively.

The stabilisation of lifted non-premixed flames has been characterised previously [7,54], which details the theory of a competing relationship between the local gas velocity and flame propagation speed, with the flame base stabilising where these two properties are equal. As highlighted in Section 1, the axial component of gas velocity is reduced with the addition of swirl. This extends the blow-off limit and permits a larger heat input which is desirable in many industrial applications. Similarly, increasing the propagation rate or burning velocity can also increase stability. The burning velocity of a stoichiometric methane mixture is increased dramatically by blending with hydrogen, increasing from 0.25 m/s to 2.9 m/s — however, this increase is non-linear and is

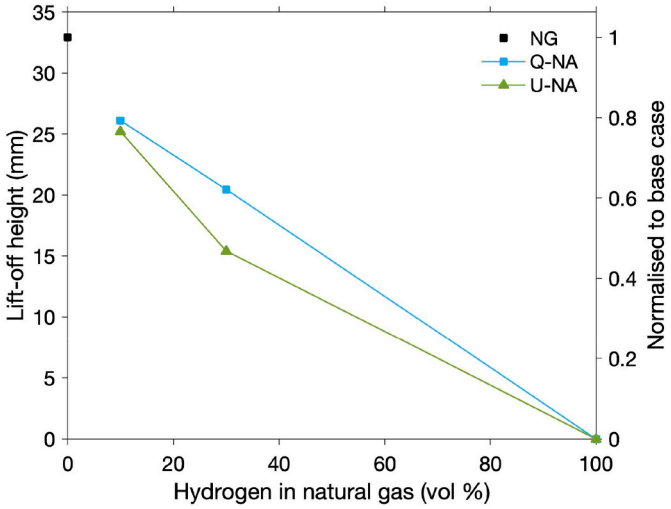

Fig. 4. Flame lift-off height determined from OH* images for hydrogen addition to natural gas (NG) at constant heat input (Q-NA) and constant jet velocity (U-NA) – refer Table 1. The volumetric flow rate of swirled co-annular air is maintained in both instances.

only small for weak blends of hydrogen in methane [55]. The implications of this effect on burning velocity are the most likely cause for the observed discrepancy in lift-off height from 10 to 30 vol% hydrogen when jet velocity is conserved, as shown in Fig. 4. Note also that the reduction in lift off height is less significant in the constant heat input cases compared with the constant velocity cases. As mentioned previously, this is a result of an increase in volumetric flow rate of fuel which increases velocity as hydrogen is added (due to its lower volumetric energy density). In either case, at 100 % hydrogen, the flames are observed to completely reattach to the burner. An attached flame may result in increased burner surface temperature but would also mean increased resistance to blow-off. This would allow for a much higher heat input to be achieved while avoiding extinction, a desirable feature for industrial combustion applications.

3.2. Radiative heat transfer

Quantifying the degree to which the displacement of hydrocarbon-based fuels impacts heat transfer is a vital step in the de-risking of alternative fuels such as hydrogen. Fig. 5 shows the axial heat flux profile for hydrogen addition to natural gas at either constant heat input (top) or constant velocity (bottom) from 0 to 1200 mm above the burner.

The axial heat flux profiles of almost all flames takes a similar shape, reaching a maximum at ~500 mm above the burner which correlates with the location of maximum flame width observed in Fig. 2. Similarly, heat flux approaches zero towards 1200 mm above the burner, consistent with the visual flame heights presented in Fig. 2. A qualitative observation can also be made that the flame images which appeared the most luminous were also the most radiant, consistent with the assumption that soot is the primary cause for radiant heat transfer and luminosity.

The effects of hydrogen addition were dependent on whether heat input or velocity were conserved. For constant heat input cases, the influence of hydrogen addition on the magnitude and shape of the heat flux profiles was negligible up to 30 vol%. For 100 % hydrogen, a reduction of almost 30 % in radiant heat flux was observed on average across the full length of the flame, compared with natural gas. Since heat input is conserved for these cases, any reductions in radiative heat release are attributed to the displacement of sooting species. As expected, lower heat flux measurements were observed for the U-NA cases compared with Q-NA cases due to the subsequent decrease in heat input.

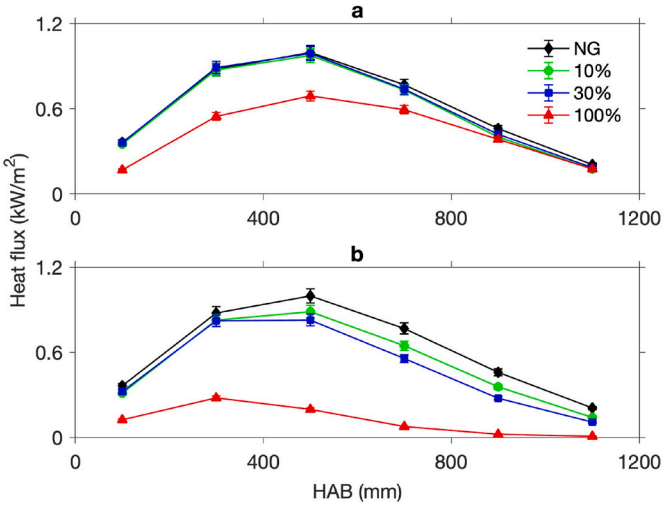

Fig. 5. Axial heat flux measurements for hydrogen addition to natural gas (NG) at for constant heat input (Q-NA) (a) and for constant jet velocity (U-NA) (b) – refer Table 1. The volumetric flow rate of swirled co-annular air is maintained in both instances. The error bars represent the 0.005 % of the measured value, which is the accuracy of the measurement equipment.

To directly assess the influence of hydrogen on radiant heat transfer, the results in Fig. 5 have been converted to a radiant fraction and presented in Fig. 6 as a function of hydrogen fraction in the fuel. In this case, a closer trend between constant heat input and constant velocity cases is observed. Radiant fraction (refer Eq (2), is normalised by heat input. The radiant fraction of the natural gas base case is calculated to be 15.3 %, complete replacement of natural gas for hydrogen results in a 30–36 % reduction on overall radiant fraction, depending on if heat input or velocity were conserved when hydrogen is added. Hydrogen addition up to 10 vol% showed a minor (4–7%) reduction in radiant fraction — but 30 vol% hydrogen showed only a 0–2% reduction.

Since radiant fraction is normalised by heat input, it can be used to analyse the radiative capacity of a given fuel blend irrespective of its supply rate (heat input). Given the close agreement between constant heat input and velocity cases in Fig. 6, it can be inferred that the effect of hydrogen addition, or rather, of soot displacement, with respect to the radiant fraction is consistent regardless of heat input. That is, at the complete displacement of natural gas with hydrogen will lead to a 33 % reduction in the overall radiant fraction of the flame, regardless of how the supply rate is adjusted with fuel composition.

3.3. Influence of H_2 on flame temperature and NOx

A critical component of an investigation on the effects of hydrogen addition to a particular burner design is a characterisation of the effects of hydrogen on flame temperature and NOx emissions. Axial centreline temperature profiles from 0 to 1200 mm above the burner and NOx emissions in the post-flame region (2000 mm above the burner) are presented in Figs. 7 and 8, respectively.

Flue gas NOx samples for the base natural gas case are measured to be 20 mg/MJ. Hydrogen addition up to 10 vol% increases NOx emissions by as much as 25 % with a negligible distinction between whether hydrogen is added at constant heat input or constant velocity. the 30 vol % hydrogen blends produced 47 % and 31 % more NOx emissions, depending on if heat input or velocity were conserved, respectively. The 100 % hydrogen cases increased NOx emissions by a factor of 2.2 and 1.8, depending on if heat input or velocity were conserved, respectively. The influence of hydrogen addition strategy (constant heat input versus constant velocity) was not shown to significant with respect to NOx. That is, the distinction between constant heat input and constant velocity cases is insignificant.

The centreline temperature data presented in Fig. 7 shows the peak

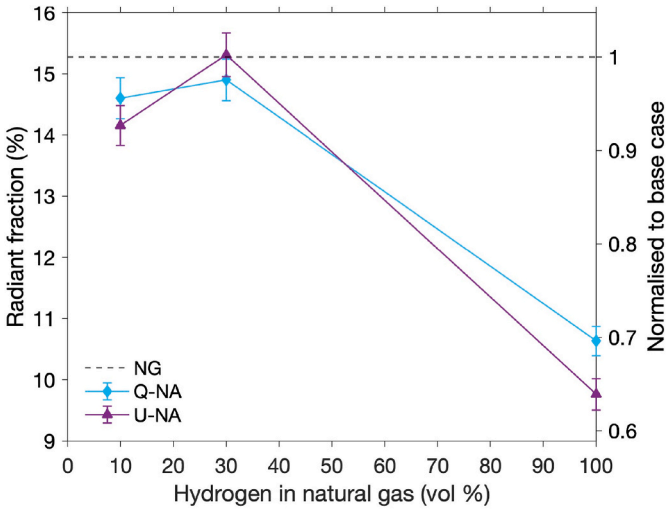

Fig. 6. Radiant heat fraction (%) for hydrogen addition to natural gas (NG) at constant heat input (Q-NA) and constant jet velocity (U-NA) – refer Table 1. The volumetric flow rate of swirled co-annular air is maintained in both instances. The error bars represent the 0.005 % accuracy of the measurement equipment.

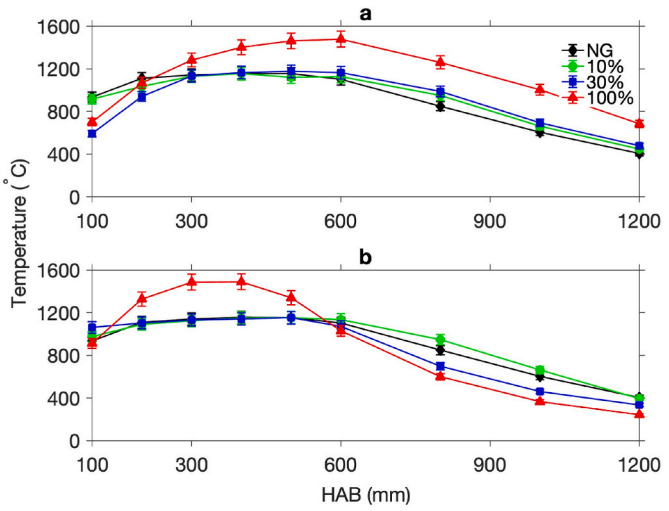

Fig. 7. Axial centreline temperature measurements for hydrogen addition to natural gas (NG) at for constant heat input (Q-NA) (a) and for constant jet velocity (U-NA) (b) – refer Table 1. The volumetric flow rate of swirled co-annular air is maintained in both instances. The error bars represent the 0.05 % of the measured value, which is the accuracy of the measurement equipment.

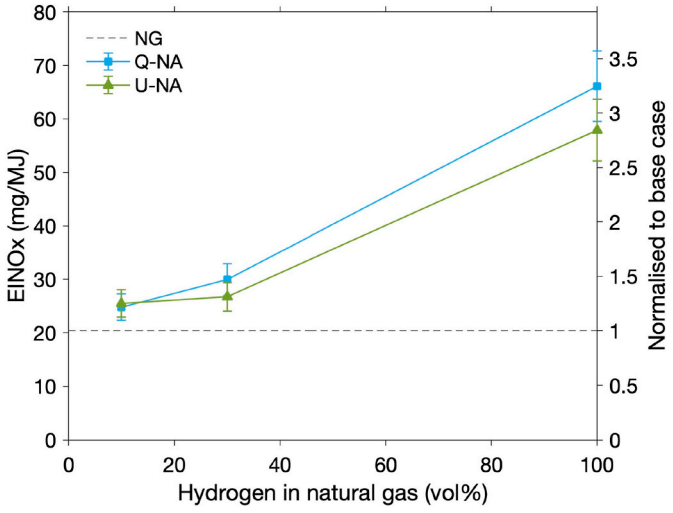

Fig. 8. Flue gas NOx measurements taken in the post-flame region (2000 mm above the burner) for hydrogen addition to natural gas (NG) at constant heat input (Q-NA) and constant jet velocity (U-NA) – refer Table 1. The volumetric flow rate of swirled co-annular air is maintained in both instances. The error bars represent the 0.1 % of the measured value, which is the accuracy range of the measurement equipment.

flame temperature, which is a good indicator of thermal NOx formation rates [56–58], is similar, varying by less than 2 % for each fuel blend, regardless of how hydrogen is added. This is consistent with the similar trends observed for NOx emissions for hydrogen addition at constant heat input and constant velocity in Fig. 8. Although hydrogen addition did not shift the location of peak flame temperature downstream, as reported in previous work [8], it is noteworthy that the location of peak flame temperature is shifted upstream toward the burner for constant velocity cases compared to constant heat input. The reduction in fuel flow to conserve velocity as hydrogen is added shortens flame length, as discussed in Section 3.1. This shortening of overall flame length causes the peak flame temperature to shift upstream. As discussed in Section 3.2, it is concluded the fuel-air mixing is more intense closer to the burner. A peak flame temperature closer to the region where air (the source of nitrogen) is most effectively mixed with the fuel may also contribute to NOx emissions and is further discussed is Section 3.4.

3.4. *Influence of swirled co-annular air*

Changing the properties of the fuel stream with no adjustment of the air supply, such as the cases discussed in Section 3.1-3.3, can result in large changes in the parameters which are fundamental to a swirl burner operation. This section (Section 3.4) considers the implications of hydrogen addition under conditions where the fuel/air momentum flux ratio or equivalence ratio have been conserved. In particular, co-annular air was adjusted to conserve either fuel/air momentum ratio (Q-MF and U-MF) or equivalence ratio (Q-ER and U-ER) as hydrogen fraction is varied. A more detailed description of the flame cases is presented in Table 1. By comparing the effects of co-annular air supply via its associated parameters (equivalence ratio and fuel/air momentum flux ratio) a more complete characterisation of the effects of hydrogen addition to the burner can be achieved.

The adjustment of co-annular air to conserve either fuel/air momentum flux ratio or equivalence ratio did not significantly impact the flame appearance hence, DSLR and OH* chemiluminescence images have been presented separately in the Supplementary Material. To visualise how momentum flux ratio and equivalence ratio vary between flame cases and to quantify their impact on performance, the data in this section are presented as a function of momentum flux ratio or equivalence ratio. Specific flame cases are distinguished using different formatting as outlined in the respective figure legends.

The mixing and stability of swirl burner flames is heavily dependent on fuel and air supply and specifically on the fuel and air momentum flux ratio [36,59]. Fundamental stability metrics such as lift-off height can be significantly affected by subtle changes in fuel properties or supply ratios with co-annular air. As a result, it is important to characterise how changes in fuel/air momentum flux affect these metrics. The lift-off height, as determined from the OH* chemiluminescence images in Fig. 3, Fig. S2 and Fig. S7, is presented in Fig. 9 as a function of momentum flux ratio and equivalence ratio.

The results from Fig. 9 show a correlation between hydrogen fraction and lift-off height, with distinction between 10, 30 and 100 % hydrogen flames being apparent. The 10 vol% hydrogen flames were all lifted 25–30 mm above the burner, a 9–24 % reduction in the lift-off height relative to the base natural gas case. The 30 vol% flames were less lifted than the 10 vol% flames but more distributed, with lift-off heights varying between 13 and 20 mm observed, a 39–61 % reduction in lift-off height compared with the base case. Finally, all pure hydrogen flames were observed to be attached to the burner.

The data points in Fig. 9 are clustered, primarily by fuel composition (hydrogen fraction) and heat input. As discussed in Section 3.1, it is expected that a reduction in axial velocity will contribute to reducing lift-off height and an eventual anchoring of the flame to the burner. Similarly, changes in fuel composition which increase burning velocity are also expected to decrease lift-off height. This is consistent with the observations presented in Fig. 9. Cases which conserve heat input have a higher volumetric flow rate of fuel and as a result, are lifted more than lower heat input cases. This is most clearly seen for the 30 vol% hydrogen cases, where for a 26 % increase in velocity, the 97 kW cases are 25 % more lifted than 77 kW cases.

The fuel/air momentum flux ratio has been shown to be a dictating parameter of co-annular swirl burner flames [36,59], however, in this case, no clear correlation could be drawn between lift-off height and fuel/air momentum flux ratio. A minor decrease in lift-off height is observed for the 30 vol% hydrogen (constant velocity) cases as co-annular air supply is reduced but this observation could not be observed for other cases.

To understand the role of fuel composition on thermal radiation, radiant heating fractions for each flame are presented as functions of momentum flux ratio and equivalence ratio in Fig. 10.

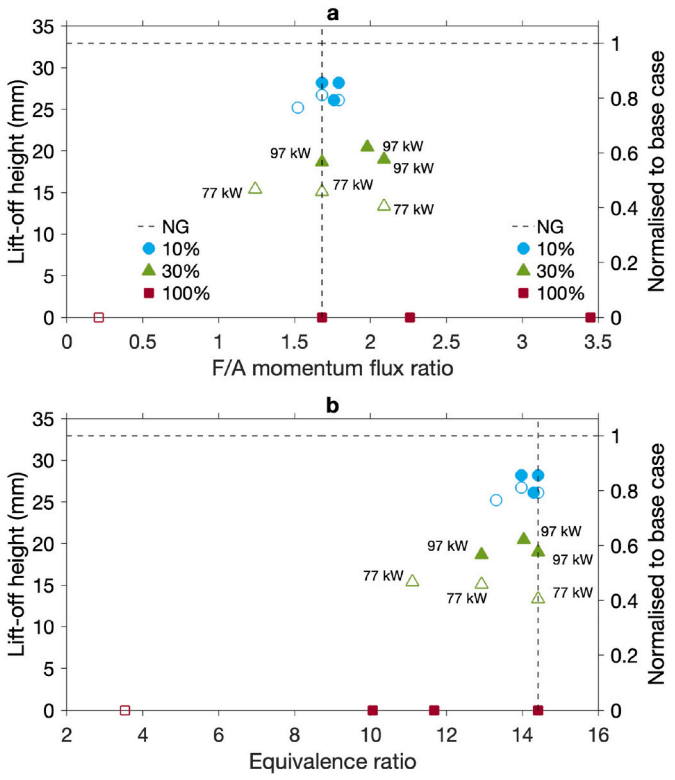

Fig. 9. Flame lift-off height extracted from chemiluminescence images presented as a function of fuel/air momentum flux ratio (a) and equivalence ratio (b). Constant heat input (Q-) and constant velocity cases (U-) are identified with filled and open markers, respectively. Lift-off height is defined as the point along the axial centreline from the burner exit to the flame at which OH* chemiluminescence intensity reaches 15 % of the flame's peak intensity. 30 vol % H_2 data points have been annotated to show their respective heat inputs.

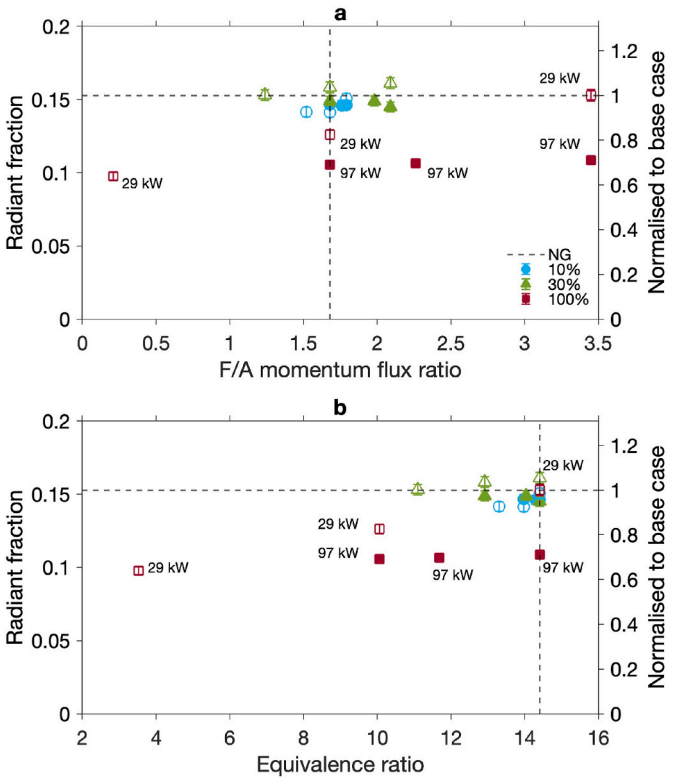

Fig. 10. Radiant heat fraction for hydrogen addition to natural gas (NG) in a co-annular swirl burner for various fuel/air momentum flux (a) and equivalence ratios (b). Constant heat input (Q-) and constant velocity cases (U-) are identified with filled and open markers, respectively. The data points for pure hydrogen flames have been annotated to also include their respective heat inputs. The error bars represent the 0.005 % of the measured value, which is the accuracy of the measurement equipment.

The results in Fig. 10 show a similar observation to that discussed in Section 3.2. That is, there is a clear reduction in radiant fraction by complete substitution of natural gas for hydrogen. The distinction between natural gas and the 10 and 30 vol% hydrogen mixtures is less significant, regardless of co-annular air supply.

For the 10 and 30 vol% blends presented in Fig. 10, minor changes in radiant fraction relative to the base natural gas case are observed but no clear correlation between is apparent — noting that radiant fraction accounts for heat input and so variation due to supply rate is eliminated. There is, however, a positive relationship between radiant fraction and both momentum flux ratio and equivalence ratio (i.e. with decreasing the air supply). This observation is most pronounced in the pure hydrogen cases where velocity is conserved (i.e. for 100 % H_2 29 kW cases) but can also be seen to a lesser extent in the 10 and 30 vol% blends. Momentum flux ratio and equivalence ratio are increased from 0.21 to 3.53, to 3.45 and 14.41, respectively, radiant heating fraction for the 29 kW pure hydrogen cases increases linearly ($R^2 = 0.99$) by up to 57 % for the 100 % hydrogen cases.

A reduction in air supply would typically result in an increase in soot formation, leading to increased radiant heat transfer. However, for pure hydrogen cases where there is no carbon present this cannot be the cause. Instead, it is likely that by reducing the flow rate of gas exiting the burner, the entrainment of surrounding secondary air is reduced which may have been contributing a diluting/cooling effect, lowering the heat release. This would also explain why the effect is not observed for the 97 kW cases, which have a much higher flow rate of fuel and therefore entrain a greater volume of dilution air.

An increase in flame dilution would be expected to impact other factors, such as thermal NOx production. The interactions between fuel and air in a co-annular swirl burner have the potential to influence local temperature zones and resulting thermal NOx emissions. To investigate and characterise these effects, the changes in NOx emissions with respect to fuel/air momentum flux ratio and equivalence ratio are presented in Fig. 11.

Overall, the results from Fig. 11 suggest fuel/air momentum flux ratio does not have a consistent impact on NOx emissions for a given fuel blend. For most fuel blends, any changes in NOx emissions are too small to be evidence of any correlation with momentum flux. The highest increase in NOx emissions relative to the base case was for pure hydrogen at constant velocity, producing 4.8-times more NOx than the natural gas base case — this is also the case which has the peak centreline flame temperature occurring closest to the burner exit, as shown in Fig. S9 in the Supplementary Material. This observation further supports the hypothesis made in Section 3.3. That is, the fuel and air mixing is presumed to be strongest nearer to the burner and a region in which maximum fuel-air mixing and peak flame temperature are occurring creates an environment for increased thermal NOx formation.

The results in Fig. 11 show that for hydrogen addition at 29 kW (constant velocity), decreasing swirled co-annular air supply increases NOx emissions. The observation is partially observed for 97 kW (constant heat input) cases but cannot be observed for other fuel blends. Decreasing co-annular air supply may contribute to reducing NOx emissions by reducing fuel/air mixing close to the burner exit and shifting the location of peak flame temperature downstream, where fuel/air mixing is poorer. Furthermore, by reducing the primary swirled air supply, a greater amount of secondary air must be entrained in the downstream portion of the flame to sustain the reaction.

The effect of conserving heat input versus velocity appears negligible

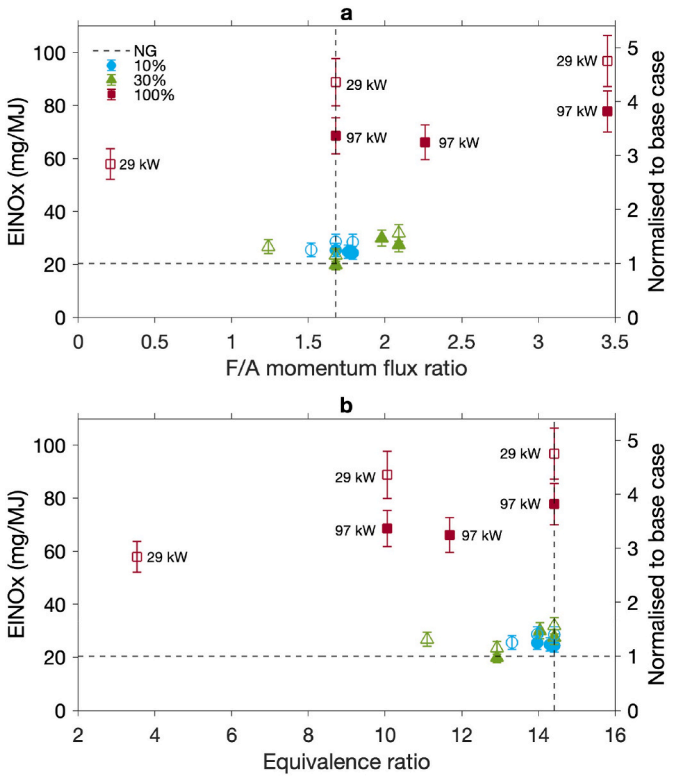

Fig. 11. Flue gas NOx measurements taken in the post-flame region (2000 mm above the burner) for hydrogen addition to natural gas (NG) in a co-annular swirl burner for various fuel/air momentum flux (a) and equivalence ratios (b). Constant heat input (Q-) and constant velocity cases (U-) are identified with filled and open markers, respectively. The data points for pure hydrogen flames have been annotated to also include their respective heat inputs. The error bars represent the 0.1 % of the measured value, which is the accuracy of the measurement equipment.

with respect to its impact on the normalised NOx emissions in the flue gas. This is explained by the consistent peak flame temperatures for each fuel blend. Any variation in NOx with heat input can be explained by a changing of the mixing intensity and location of the peak flame temperature, as a result of the fuel and air flow ratios. This observation is significant as it may allow for a strategic adjustment of fuel and air supply to mitigate the increased NOx emissions as a result of hydrogen addition. This would be a simple and cost-effective solution strategy compared with, for example, changing the vane angles of the nozzle, which would require a complete redesign and replacement of the burner.

The mixed sensitivity to co-annular air with respect to stability, radiant heat transfer and NOx is most likely a consequence of the non-premixed and low-swirl nature of the flames tested in this investigation. For applications where the flames are stabilised by different mechanisms within the swirl structures, such as premixed and/or HSB flames, fluctuations in equivalence ratio or momentum flux may have a different effect. In general, it could be said that non-premixed and low-swirl burners are well suited for use with hydrogen-natural gas due to the high turn-down capacity, relatively low impact of hydrogen as lower blend ratios and the capacity for simple and cost-effective adjustments at higher blend ratios. Furthermore, the increase stability gained by operating with hydrogen, even at low blending ratios, can be considered an improved feature which may be desirable in many industrial applications and for many future fuel opportunities such as operating with biogas.

4. Conclusions

The performance of a scaled industrial co-annular LSB design was investigated for various non-premixed turbulent hydrogen-natural gas flames up to 100 % hydrogen. Hydrogen was added conserving either heat input or velocity. Additionally, the influence of co-annular air was investigated via three different approaches for the change in fuel blend: co-annular air was either left unadjusted (constant volumetric flow), adjusted to conserve fuel/air momentum flux ratio or adjusted to conserve equivalence ratio as the fuel blend changed. Four key findings may be summarised as:

1. The visual distinctions were mostly negligible for 10 and 30 vol% hydrogen addition with only small reductions in visible flame length. No colour or luminosity changes were observed up to 30 vol% hydrogen. Complete replacement of natural gas with hydrogen resulted in a shorter and narrower flame that was almost invisible to the naked eye. There was no noteworthy distinction between hydrogen addition at constant heat input versus constant velocity, except for a reduction in flame size due to the difference in volumetric flow rate.
2. The characteristic lifted flames of a LSB were shown to decrease their lifted height from the burner both as hydrogen concentration increased and as heat input decreased. Hydrogen addition of 10 % and 30 % reduced lift-off height by 9–24 % and 39–61 %, respectively, depending on how/if co-annular air was adjusted. At 100 % hydrogen the flames became attached to the burner. The cause for this was determined to be an increase in burning velocity due to hydrogen and a decrease in burner fuel exit velocity as heat input decreased.
3. Hydrogen addition had a negligible effect on the radiant heat transfer properties of the flames for the 10 and 30 vol%. Complete substitution of natural gas for hydrogen caused a 33 % reduction in the fraction of radiant heat generated from the flames that was consistent regardless of whether hydrogen was blended at constant heat input or constant velocity. This was deemed to be a result of soot displacement.
4. Hydrogen addition caused an increase in NOx emissions along the flame centreline in the post-flame region, most notably for the 100 % hydrogen case. Addition of 10 % and 30 % hydrogen increased NOx emissions by up to 25 % and 47 %, respectively. Compete substitution of natural gas for hydrogen resulted in up to 4.8-fold increase in NOx emissions. Conserving velocity compared to heat input had a negligible effect of magnitude of peak flame temperature but did cause a shift in location of peak flame temperature upstream toward the burner. The influence of co-annular air adjustment become more significant as hydrogen fraction increased. This highest NOx emissions were recorded for the constant velocity hydrogen addition and lowest co-annular air supply. NOx emissions could be reduced by increased fuel flow rate and increased co-annular air supply — this may be a potential simple and low-cost approach to mitigating the high NOx emissions associated with hydrogen flames.

Declaration of competing interest

The authors declare that they have no known competing financial interests or personal relationships that could have appeared to influence the work reported in this paper.

Acknowledgements

The authors acknowledge the support from the Australian Research Council, The University of Adelaide and the Future Fuels CRC. The authors also thank Ben Crossman and Douglas Proud for their support.

Appendix A. Supplementary data

Supplementary data to this article can be found online at https://doi.org/10.1016/j.ijhydene.2023.11.164.

References

[1] An Q, Kheirkhah S, Bergthorson J, Yun S, Hwang J, Lee WJ, Kim MK, Cho JH, Kim HS, Vena P. Flame stabilization mechanisms and shape transitions in a 3D printed, hydrogen enriched, methane/air low-swirl burner. Int J Hydrogen Energy 2021;46(27):14764–79. https://doi.org/10.1016/j.ijhydene.2021.01.112.

[2] Candel S, Durox D, Schuller T, Bourgouin J-F, Moeck JP. Dynamics of swirling flames. Annu Rev Fluid Mech 2014;46(1):147–73. https://doi.org/10.1146/annurev-fluid-010313-141300.

[3] Saqib M, Shahsavari M, Ghosh A, Wang B, Hussain Z, Rao Z. Effect of fuel reactivity on flame properties of a low-swirl burner. Exp Therm Fluid Sci 2023;142:110795. https://doi.org/10.1016/j.expthermflusci.2022.110795.

[4] Lucca-Negro O, O'Doherty T. Vortex breakdown: a review. Prog Energy Combust Sci 2001;27(4):431–81. https://doi.org/10.1016/S0360-1285(00)00022-8.

[5] Syred N, Chigier NA, Beér JM. Flame stabilization in recirculation zones of jets with swirl. Symposium (International) on Combustion 1971;13(1):617–24. https://doi.org/10.1016/S0082-0784(71)80063-2.

[6] Jiang X, Luo KH, de Goey LPH, Bastiaans RJM, van Oijen JA. Swirling and impinging effects in an annular nonpremixed jet flame. Flow, Turbul Combust 2011;86(1):63–88. https://doi.org/10.1007/s10494-010-9287-y.

[7] Navarro-Martinez S, Kronenburg A. Flame stabilization mechanisms in lifted flames. Flow, Turbul Combust 2011;87(2):377–406. https://doi.org/10.1007/s10494-010-9320-1.

[8] Cellek MS, Pınarbaşı A. Investigations on performance and emission characteristics of an industrial low swirl burner while burning natural gas, methane, hydrogen-enriched natural gas and hydrogen as fuels. Int J Hydrogen Energy 2018;43(2):1194–207. https://doi.org/10.1016/j.ijhydene.2017.05.107.

[9] Cozzi F, Coghe A. Behavior of hydrogen-enriched non-premixed swirled natural gas flames. Int J Hydrogen Energy 2006;31(6):669–77. https://doi.org/10.1016/j.ijhydene.2005.05.013.

[10] Restrepo A, Viana M, Colorado A, Amell AA. Experimental investigation of hydrogen enriched natural gas diffusion reactions using preheated air in a hot coflow burner. Int J Hydrogen Energy 2023;48(1):337–49. https://doi.org/10.1016/j.ijhydene.2022.09.232.

[11] Rahimi S, Mazaheri K, Alipoor A, Mohammadpour A. The effect of hydrogen addition on methane-air flame in a stratified swirl burner. Energy 2023;265:126354. https://doi.org/10.1016/j.energy.2022.126354.

[12] Pessoa-Filho JB. Thermal radiation in combustion systems. J Braz Soc Mech Sci 1999;21(3):537–47. https://doi.org/10.1590/S0100-73861999000300014.

[13] Hamadi MB, Vervisch P, Coppalle A. Radiation properties of soot from premixed flat flame. Combust Flame 1987;68(1):57–67. https://doi.org/10.1016/0010-2180(87)90065-4.

[14] Hutny WP, Lee GK. Improved radiative heat transfer from hydrogen flames. Int J Hydrogen Energy 1991;16(1):47–53. https://doi.org/10.1016/0360-3199(91)90059-R.

[15] Saito K, Williams FA, Gordon AS. Effects of oxygen on soot formation in methane diffusion flames. Combust Sci Technol 1986;47(3–4):117–38. https://doi.org/10.1080/00102208608923869.

[16] Sen S, Puri I. Thermal radiation modeling in flames and fires. Transport Phenonema in Fires; 2008. p. 301.

[17] Schiro F, Stoppato A, Benato A. Modelling and analyzing the impact of hydrogen enriched natural gas on domestic gas boilers in a decarbonization perspective. Carbon Res Convers 2020;3:122–9. https://doi.org/10.1016/j.crcon.2020.08.001.

[18] Gee AJ, Yin Y, Foo KK, Chinnici A, Smith N, Medwell PR. Toluene addition to turbulent H2/natural gas flames in bluff-body burners. Int J Hydrogen Energy 2022;47(65):27733–46. https://doi.org/10.1016/j.ijhydene.2022.06.154.

[19] Tangirala V, Chen RH, Driscoll JF. Effect of heat release and swirl on the recirculation within swirl-stabilized flames. Combust Sci Technol 1987;51(1–3):75–95. https://doi.org/10.1080/00102208708960316.

[20] Tangirala V, Driscoll JF. Temperatures within non-premixed flames: effects of rapid mixing due to swirl. Combust Sci Technol 1988;60(1–3):143–62. https://doi.org/10.1080/00102208808923981.

[21] Yang X, Zhao L, He Z, Dong S, Tan H. Comparative study of combustion and thermal performance in a swirling micro combustor under premixed and non-premixed modes. Appl Therm Eng 2019;160:114110. https://doi.org/10.1016/j.applthermaleng.2019.114110.

[22] Huang Y, Yang V. Dynamics and stability of lean-premixed swirl-stabilized combustion. Prog Energy Combust Sci 2009;35(4):293–364. https://doi.org/10.1016/j.pecs.2009.01.002.

[23] Elbaz AM, Mannaa O, Roberts WL. Flame flow field interaction in non-premixed CH4/H2 swirling flames. Int J Hydrogen Energy 2021;46(59):30494–509. https://doi.org/10.1016/j.ijhydene.2021.06.176.

[24] Lahaye D, Abbassi Me, Vuik K, Talice M, Juretić F. Mitigating thermal NOx by changing the secondary air injection channel: a case study in the cement industry. Fluid 2020;5(4):220. https://doi.org/10.3390/fluids5040220.

[25] Abbassi M, Lahaye D, Vuik C. The effect of variable air–fuel ratio on thermal NOx emissions and numerical flow stability in rotary kilns using non-premixed combustion. Processes 2021;9(10):1723. https://doi.org/10.3390/pr9101723.

[26] Hosseini AA, Ghodrat M, Moghiman M, Pourhoseini SH. Numerical study of inlet air swirl intensity effect of a Methane-Air Diffusion Flame on its combustion characteristics. Case Stud Therm Eng 2020;18:100610. https://doi.org/10.1016/j.csite.2020.100610.

[27] Yilmaz İ, Ratner A, Ilbas M, Huang Y. Experimental investigation of thermoacoustic coupling using blended hydrogen–methane fuels in a low swirl burner. Int J Hydrogen Energy 2010;35(1):329–36. https://doi.org/10.1016/j.ijhydene.2009.10.018.

[28] Ranga Dinesh KKJ, Luo KH, Kirkpatrick MP, Malalasekera W. Burning syngas in a high swirl burner: effects of fuel composition. Int J Hydrogen Energy 2013;38(21):9028–42. https://doi.org/10.1016/j.ijhydene.2013.05.021.

[29] Ge B, Ji Y, Zhang Z, Zang S, Tian Y, Yu H, Chen M, Jiao G, Zhang D. Experiment study on the combustion performance of hydrogen-enriched natural gas in a DLE burner. Int J Hydrogen Energy 2019;44(26):14023–31. https://doi.org/10.1016/j.ijhydene.2019.03.257.

[30] Oztarlik G, Selle L, Poinsot T, Schuller T. Suppression of instabilities of swirled premixed flames with minimal secondary hydrogen injection. Combust Flame 2020;214:266–76. https://doi.org/10.1016/j.combustflame.2019.12.032.

[31] Schefer RW, Wicksall DM, Agrawal AK. Combustion of hydrogen-enriched methane in a lean premixed swirl-stabilized burner. Proc Combust Inst 2002;29(1):843–51. https://doi.org/10.1016/S1540-7489(02)80108-0.

[32] Oh J, Hwang J, Yoon Y. EINOx scaling in a non-premixed turbulent hydrogen jet with swirled coaxial air. Int J Hydrogen Energy 2010;35(16):8715–22. https://doi.org/10.1016/j.ijhydene.2010.04.159.

[33] Kim S-H, Yoon Y, Jeung I-S. Nitrogen oxides emissions in turbulent hydrogen jet non-premixed flames: effects of coaxial air and flame radiation. Proc Combust Inst 2000;28(1):463–71. https://doi.org/10.1016/S0082-0784(00)80244-1.

[34] Laera D, Agostinelli PW, Selle L, Cazères Q, Oztarlik G, Schuller T, Gicquel L, Poinsot T. Stabilization mechanisms of CH4 premixed swirled flame enriched with a non-premixed hydrogen injection. Proc Combust Inst 2021;38(4):6355–63. https://doi.org/10.1016/j.proci.2020.06.378.

[35] Péquin A, Evans MJ, Chinnici A, Medwell PR, Parente A. The reactor-based perspective on finite-rate chemistry in turbulent reacting flows: a review from traditional to low-emission combustion. Appl Energy Combus Sci 2023;16:100201. https://doi.org/10.1016/j.jaecs.2023.100201.

[36] Cheng TS, Chao YC, Wu DC, Yuan T, Lu CC, Cheng CK, Chang JM. Effects of fuel-air mixing on flame structures and NOx emissions in swirling methane jet flames. Symposium (International) on Combustion 1998;27(1):1229–37. https://doi.org/10.1016/S0082-0784(98)80527-4.

[37] Schefer RW, Kulatilaka WD, Patterson BD, Settersten TB. Visible emission of hydrogen flames. Combust Flame 2009;156(6):1234–41. https://doi.org/10.1016/j.combustflame.2009.01.011.

[38] Zhao Y, Soto Leytan KN, McDonell V, Samuelsen S. Investigation of visible light emission from hydrogen-air research flames. Int J Hydrogen Energy 2019;44(39):22347–54. https://doi.org/10.1016/j.ijhydene.2019.06.105.

[39] Gee AJ, Proud DB, Smith N, Chinnici A, Medwell PR. Hydrogen addition to a commercial self-aspirating burner and assessment of a practical burner modification strategy to improve performance. Int J Hydrogen Energy 2023. https://doi.org/10.1016/j.ijhydene.2023.06.230.

[40] Robinson JW, Smith V. Emission spectra of organic liquids in oxy-hydrogen flames. Anal Chim Acta 1966;36:489–98. https://doi.org/10.1016/0003-2670(66)80084-3.

[41] Arens EE, Youngquist RC, Starr SO. Intensity calibrated hydrogen flame spectrum. Int J Hydrogen Energy 2014;39(17):9545–51. https://doi.org/10.1016/j.ijhydene.2014.04.043.

[42] Bergstrand P, Försth M, Denbratt I. The influence of orifice diameter on flame lift-off length, vol. 9; 2002. p. 11. https://doi.org/10.1007/s12239-022-0044-8. Zaragoza.

[43] Siebers D, Higgins B. Effects of injector conditions on the flame lift-off length of DI diesel sprays. In: Thermo-and fluid-dynamic processes in diesel engines: selected papers from the thiesel 2000 conference held in Valencia, Spain; 2000. 13–15, 2000.

[44] Xie F, Yang J, Wei J, Wu R, Song X, Wang J, Yu G. Investigation of the OH* chemiluminescence characteristics in CH4/O2 lifted flames. J Energy Inst 2021;99:31–8. https://doi.org/10.1016/j.joei.2021.08.007.

[45] Buch R, Hamins A, Konishi K, Mattingly D, Kashiwagi T. Radiative emission fraction of pool fires burning silicone fluids. Combust Flame 1997;108(1):118–26. https://doi.org/10.1016/S0010-2180(96)00098-3.

[46] Langman AS, Nathan GJ, Mi J, Ashman PJ. The influence of geometric nozzle profile on the global properties of a turbulent diffusion flame. Proc Combust Inst 2007;31(1):1599–607. https://doi.org/10.1016/j.proci.2006.07.165.

[47] Dong X, Nathan GJ, Mahmoud S, Ashman PJ, Gu D, Dally BB. Global characteristics of non-premixed jet flames of hydrogen–hydrocarbon blended fuels. Combust Flame 2015;162(4):1326–35. https://doi.org/10.1016/j.combustflame.2014.11.001.

[48] Brohez S, Delvosalle C, Marlair G. A two-thermocouples probe for radiation corrections of measured temperatures in compartment fires. Fire Saf J 2004;39(5):399–411. https://doi.org/10.1016/j.firesaf.2004.03.002.

[49] Abdel-Aal HK, Sadik M, Bassyouni M, Shalabi M. A new approach to utilize Hydrogen as a safe fuel. Int J Hydrogen Energy 2005;30(13):1511–4. https://doi.org/10.1016/j.ijhydene.2005.07.007.

[50] Yin Y, Medwell PR, Gee AJ, Foo KK, Dally BB. Fundamental insights into the effect of blending hydrogen flames with sooting biofuels. Fuel 2023;331:125618. https://doi.org/10.1016/j.fuel.2022.125618.

[51] Gore JP, Zhan NJ. NOx emission and major species concentrations in partially premixed laminar methane/air co-flow jet flames. Combust Flame 1996;105(3):414–27. https://doi.org/10.1016/0010-2180(95)00177-8.
[52] Attia A, Ayoub H, Ghazolin B, El-Sherief A, El-Gohary M, Emara A, Moneib H, Elbashar Y. In-Situ Soot visualization using Low power 405nm laser shadowgraphy for premixed and non-premixed flames. Anna; Univ Craiova, Phys 2018;28:12–6.
[53] Olivani A, Solero G, Cozzi F, Coghe A. Near field flow structure of isothermal swirling flows and reacting non-premixed swirling flames. Exp Therm Fluid Sci 2007;31(5):427–36. https://doi.org/10.1016/j.expthermflusci.2006.05.003.
[54] Driscoll JF, Rasmussen CC. Correlation and analysis of blowout limits of flames in high-speed airflows. J Propul Power 2005;21(6):1035–44.
[55] Ilbas M, Crayford A, Yilmaz I, Bowen P, Syred N. Laminar-burning velocities of hydrogen–air and hydrogen–methane–air mixtures: an experimental study. Int J Hydrogen Energy 2006;31(12):1768–79. https://doi.org/10.1016/j.ijhydene.2005.12.007.
[56] Kotb A, Saad H. A comparison of the thermal and emission characteristics of co and counter swirl inverse diffusion flames. Int J Therm Sci 2016;109:362–73. https://doi.org/10.1016/j.ijthermalsci.2016.06.015.
[57] İlbas M, Yılmaz İ, Kaplan Y. Investigations of hydrogen and hydrogen–hydrocarbon composite fuel combustion and NOx emission characteristics in a model combustor. Int J Hydrogen Energy 2005;30(10):1139–47. https://doi.org/10.1016/j.ijhydene.2004.10.016.
[58] Skottene M, Rian KE. A study of NOx formation in hydrogen flames. Int J Hydrogen Energy 2007;32(15):3572–85. https://doi.org/10.1016/j.ijhydene.2007.02.038.
[59] Solero G, Coghe A. Effect of injection typology on turbulent homogeneous mixing in a natural gas swirl burner. Exp Therm Fluid Sci 2000;21(1):162–70. https://doi.org/10.1016/S0894-1777(99)00067-9.